Langmuir
Article
pubs.acs.org/Langmuir

Structure and Properties of Functionalized Bithiophenesilane Monodendrons

Ray Gunawidjaja,[†] Yuriy N. Luponosov,[‡] Feifei Huang,[†] Sergei A. Ponomarenko,[‡] Aziz M. Muzafarov,[‡] and Vladimir V. Tsukruk*,[†]

[†]*School of Materials Science and Engineering, Georgia Institute of Technology, Atlanta, Georgia 30332-0245, and* [‡]*Enikolopov Institute of Synthetic Polymer Materials of the RAS, Profsoyuznaya 70, Moscow, Russia*

Received March 4, 2009. Revised Manuscript Received April 9, 2009

This study reports a focal group modification of bithiophenesilane monodendrons and its effect on their molecular ordering in solution, bulk, and surface. We investigated hydrophobic MD*n* monodendrons and COOH-functionalized MD*n*−COOH monodendrons with generations, $n = 0$, 1, 2, and 3. We observed that increasing the number of branches led to the progressive blue shift, indicating distorted packing of branched thiophene fragments of MD*n*. In contrast, MD*n*−COOH monodendrons showed a progressive red shift with the increasing generation number, indicating gradual domination of $\sigma-\pi$ interactions. Moreover, the introduction of a focal carboxylic group resulted in the formation of a highly crystalline state for the linear MD0−COOH compound with separated alkyl tail−thiophene packing, which limits $\pi-\pi$ interactions. Increasing branching in the COOH-containing monodendrons resulted in a hydrophobic−hybrophilic balance sufficient to form stable and uniform Langmuir monolayers at the air−water at a modest surface pressure (< 10 mN/m), easily transferrable to a solid substrate. However, a further increase in the thickness of the surface layers from tens to hundreds of nanometers via Langmuir−Blodgett (LB) deposition or spin casting is limited by the formation of globular surface aggregates because of strong intermolecular interactions. A modest red shift observed for condensed Langmuir monolayers indicates densification of thiophene branches and limited intramonolayer crystallization, which preserves photoluminescence. In contrast, thicker surface films showed a significant red shift, confirming a dense molecular packing with strong $\pi-\pi$ interactions, which results in photoluminescence quenching.

Introduction

Thin-film organic semiconducting materials are considered for prospective applications in microelectronic devices, including organic light-emitting diodes (OLEDs) and field-effect transistors.[1] This is because of their low cost, ease of fabrication, wide-viewing angle, and low power consumption, in contrast to inorganic light-emiting diode. The band gap of an organic semiconductor is determined by the lowest unoccupied molecular orbit (LUMO) and highest unoccupied molecular orbit (HOMO) energy bands that is tunable with molecular architecture.[2] In addition to the molecular architecture, it is well-established that control over long-range molecular orientations and local molecular packing is a prerequisite for high-performance organic-based systems, and therefore, the understanding of the structure−property relationship, especially in the solid state, is critical in the design of thin-film systems.[3] Small molecules that are comprised of rod and coil segments can assemble into unique and well-defined nanoscale assemblies that are rarely seen in regular linear molecules,[4] e.g., barrel-like, left-helical tubular, nanoribbons, spherical, cylindrical, toroidal, and microporous structures.[5] These unique assemblies with, frequently, intriguing photoluminscent properties are the result of conformational and shape mismatch between the rigid rod and flexible segments covalently bonded within a single molecule, and the driving force for assembly are weak interactions that include hydrogen bonding, electrostatic, van der Waals interactions, $\pi-\pi$ interactions, and hydrophobic−hydrophilic balance.[6]

In addition to their ability to control the assembly by means of weak interactions and molecular architectures, the rod-like segments often possess useful functionalities with intriguing photophysical and electrochemical properties. Thiophene is one example of a rigid molecular fragment that is both chemically stable and has a unique combination of properties.[7] Thiophene molecules are easy to functionalize, and depending upon the functional groups and chain architecture, these molecules can emit light across the entire visible range.[8] These compounds are mainly investigated as prospective conducting, luminescent, and sensing materials. Organic semiconductors, such as polythiophenes, are commercially appealing because of their low cost and facile processing, both of which are enabled by solution-based assembly. While unsubstituted conjugated organic oligomers have the tendency to crystallize into herringbone structures, charge mobility across a thin-film organic semiconductor might be altered when the π orbitals overlap as a result of electronic

*To whom correspondence should be addressed. E-mail: vladimir@mse.gatech.edu.

(1) Rella, R.; Siciliano, P.; Quaranta, F.; Primo, T.; Valli, L.; Schenetti, L.; Mucci, A.; Iarossi, D. *Sens. Actuators, B* **2000**, *68*, 203.
(2) McNeill, R.; Siudak, R.; Wardlaw, J. H.; Weiss, D. E. *Aust. J. Chem.* **1963**, *16*, 1056.
(3) (a) Smits, E. C. P.; Mathijssen, S. G. J.; van Hal, P. A.; Setayesh, S.; Geuns, T. C. T.; Mutsaers, K. A. H. A.; Cantatore, E.; Wondergem, H. J.; Werzer, O.; Resel, R.; Kemerink, M.; Kirchmeyer, S.; Muzafarov, A. M.; Ponomarenko, S. A.; de Boer, B.; Blom, P. W. M.; de Leeuw, D. M. *Nature* **2008**, *455*, 956. (b) Tsukruk, V. V. *Prog. Polym. Sci.* **1997**, *22*, 247.
(4) (a) Stupp, S. I. *Curr. Opin. Colloid Interface Sci.* **1998**, *3*, 20. (b) Cho, B.-K.; Kim, H.-J.; Chung, Y.-W.; Lee, B.-I.; Lee, M. *Adv. Polym. Sci.* **2008**, *12*, 138. (c) May, S. J.; Zheng, J.-G.; Wessels, B. W.; Lauhon, L. *J. Adv. Mater.* **2005**, *17*, 598.
(5) (a) Genson, K. L.; Holzmueller, J.; Ornatska, M.; Yoo, Y.-S.; Park, M.-H.; Lee, M. S.; Tsukruk, V. V. *Nano Lett.* **2006**, *6*, 435. (b) Tsukruk, V. V.; Genson, K. L.; Peleshanko, S.; Markutsya, S.; Greco, A.; Lee, M.; Yoo, Y. *Langmuir* **2003**, *19*, 495. (c) Prokhorova, S. A.; Sheiko, S. S.; Müller, M.; Ahn, C.-H.; Percec, V. *Macromol. Rapid Commun.* **1998**, *19*, 359. (d) Liu, L.; Moon, K.-S.; Gunawidjaja, R.; Lee, E.; Tsukruk, V. V.; Lee, M. S. *Langmuir* **2008**, *24*, 3930.
(6) (a) Ryu, J.-H.; Lee, M. *Struct. Bonding* **2008**, *128*, 63. (b) Lee, M.; Cho B.-K.; Zin, W.-C. *Chem. Rev.* **2001**, *101*, 3869.
(7) Barbarella, G.; Melucci, M.; Sotgiu, G. *Adv. Mater.* **2005**, *17*, 1581.
(8) Barbarella, G. *Chem.—Eur. J.* **2002**, *8*, 5072.

Scheme 1. Schematic for *n*th Generation Monodendron, where $n = 0-3$ and $x = 0$ for Hydrophobic MD*n* Monodendrons and $x =$ COOH for Amphiphilic MD*n*−COOH Monodendrons

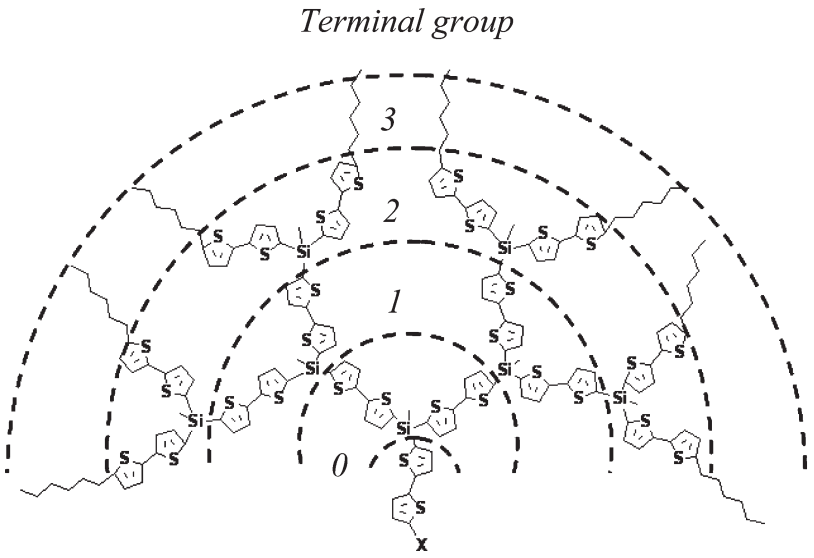

coupling between adjacent molecules, resulting in higher mobility for face−face arrangement in contrast to edge−face arrangement.[9]

Usually, nonfunctionalized polythiophene molecules are insoluble in conventional organic solvents, which makes their processing very difficult. Thus, to enhance their solubility and ability to process with conventional wet chemistry, various thiophene-based architectures have been prepared, e.g., linear, branched, oligomer, star-shaped, and all-thiophene dendrimers.[9] To this end, Reitzel et al. demonstrated that amphiphilic regioregular polythiophene derivatives at the air−water interface could adopt edge-on orientation.[10] Similarly, to obtain vertically oriented thiophenes, Senkovskyy et al. proposed to directly grow polythiopehene brush from a solid surface.[11] Conversely, in the case of OLED applications, π stacking is not desirable to avoid lowered luminescence quantum efficiency as a result of quenching[12] or undesired secondary emission.[13] Reduced π stacking is achievable in nonlinear thiophene molecules, e.g., dendrimers where the π stacking is impeded by shape persistency and multiple branching.[12c] Alternatively, bulky substituents can be introduced to inhibit a close face−face packing.[14] Longer oligothiophene fragments were found to have increased luminescent efficiency and smaller energy gaps, as a result of increased conjugation length.[15] Additionally, intermolecular conjugation is most pronounced when the molecule adapts a planar conformation.

Highly branched structures are particularly interesting because they can be tailored with multiple functionalities at their peripherals, which hence increases their solubility. Additionally, symmetrical and asymmetrical dendritic architectures can effectively provide site isolation and inhibit crystallization.[16] The number of peripheral groups or dendrimer generation can be varied to control their properties.[17] Dendrimers can also be categorized into flexible and rigid, according to their linking groups.[18] Rigid dendrimers are shape-persistent, while flexible dendrimers allow for branch folding. Their optical properties are governed by inter- and intramolecular interactions and thus depend upon their molecular ordering. It is worth noting that, although dendritic architectures have been associated with shielding of thiophene fragments, Malenfant et al. demonstrated that a functionalized polythiophene dendrimer can be conductive.[19]

Our previous studies have shown that in a dilute solution the $\sigma-\pi$ conjugation between silicon atoms and aromatic π systems of oligothiophenes in bithiophenesilane dendrimers can lead up to 30% photoluminescence quantum yield without significant change in the energy gap.[20] This value is significant compared to the parent bithiophenes that possess only 2−6% photoluminescence quantum yield. Therefore, it is of interest to elucidate their film-forming ability for a possible application in OLED devices with spin-cast and Langmuir−Blodgett (LB) techniques to be considered as a first model step in the formation of thin films on solid support.

The current study involves representatives of a recently introduced class of flexible bithiophenesilane monodendrons as well as their new chemically modified amphiphilic counterparts.[20] A monodendron is unique from dendrimer, in that, its asymmetrical shape allows for the incorporation of a focal terminal group. Here, we discuss bithiophenesilane monodendrons and functionalized COOH-containing monodendrons with generation number, $n = 0$, 1, 2, and 3 (Scheme 1). From here onward, the following notations will be used: MD*n*−COOH and MD*n* for *n*th generation carboxyl-terminated monodendrons and fully hydrophobic monodendrons, respectively (Figure 1).

The focus of this work is on understanding the role of branched architecture and focal groups on inter- and intramolecular

(9) Murphy, A. R.; Frechet, M. *J. Chem. Rev.* **2007**, *107*, 1066.
(10) Reitzel, N.; Greve, D. R.; Kjaer, K.; Howes, P. B.; Jayaraman, M.; Savoy, S.; McCullough, R. D.; McDevitt, J. T.; Bjornholm, T. *J. Am. Chem. Soc.* **2000**, *122*, 5788.
(11) Senkovskyy, V.; Khanduyeva, N.; Komber, H.; Oertel, U.; Stamm, M.; Kuckling, D.; Kiriy, A. *J. Am. Chem. Soc.* **2007**, *129*, 6626.
(12) (a) Perepichka, I. F.; Perepichka, D. F.; Meng, H.; Wudl, F. *Adv. Mater.* **2005**, *17*, 2281. (b) Taraneker, P.; Qiao, Q.; Jiang, H.; Schanze, K. S.; Reynolds, J. R. *J. Am. Chem. Soc.* **2007**, *129*, 8958. (c) Xia, C.; Fan, X.; Licklin, J.; Advincula, R. C.; Gies, A.; Nonidez, W. *J. Am. Chem. Soc.* **2004**, *126*, 8735.
(13) Takagi, K.; Momiyama, M.; Ohta, J.; Yuki, Y.; Matsuoka, S.; Suzuki, M. *Macromolecules* **2007**, *40*, 8807.
(14) Bolognesi, A.; Schieroni, A. G.; Botta, C.; Marinelli, M.; Mendichi, R.; Rolandi, R.; Relini, A.; Inganäs, O.; Theandher, M. *Synth. Met.* **2003**, *139*, 303.
(15) Bair, J. S.; Harrison, R. G. *J. Org. Chem.* **2007**, *72*, 6653.
(16) Burn, P. L.; Lo, S.-C.; Samuel, I. D. W. *Adv. Mater.* **2007**, *19*, 1675.
(17) Furuta, P.; Frechet, J. M. *J. Am. Chem. Soc.* **2003**, *125*, 13173.
(18) Zhang, Y.; Zhao, C.; Yang, J.; Kapiamba, M.; Haze, O.; Rothberg, L. J.; Ng, M.-K. *J. Org. Chem.* **2006**, *71*, 9475.
(19) Malenfant, P. R. L.; Frechet, J. M. J. *Macromolecules* **2000**, *33*, 3634.
(20) Borshchev, O. V.; Ponomarenko, S. A.; Surin, N. M.; Kaptyug, M. M.; Buzin, M. I.; Pleshkova, A. P.; Demchenko, N. V.; Myakushev, V. D.; Muzafarov, A. M. *Organometallics* **2007**, *26*, 5165.

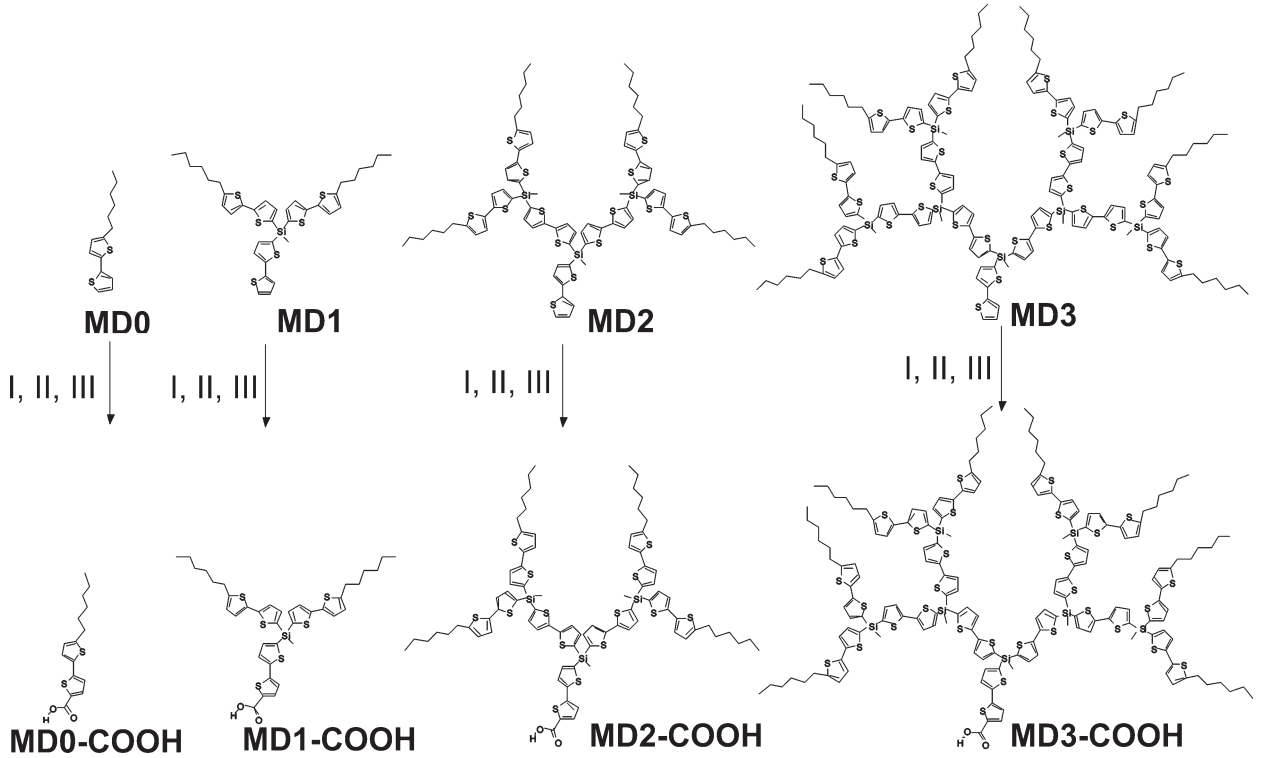

Figure 1. Synthesis and structural formulas of *n*th generation carboxyl-terminated MD*n*−COOH and fully hydrophobic bithiophenesilane monodendrons, MD*n*, with $n = 0$, 1, 2, and 3 (I = BuLi, II = CO_2, and III = HCl/H_2O).

interactions in the solid state, which in turn, govern their molecular ordering. In the solid state, the asymmetrical monodendrons are expected to root on a single end, from which *n*th generation branched molecules emanate, hence providing high-grafting density compared to their linear counterparts, while at the same time, affecting crystallization behavior and $\pi-\pi$ interactions.[21] Initially, the film-forming ability was investigated by means of spin coating. Then, the LB technique was mainly employed to systematically study the aggregation behavior. In addition, optical absorption and emission spectra were obtained to provide additional insight on their inter- and intramolecular interactions.

Experimental Section

Materials. *Chemicals*. *n*-Butyllithium (1.6 and 2.5 M solutions in hexane) (Acros Organics) and 5-hexyl-2,2′-bithiophene (Stark) were used as received. Carbon dioxide was dried by passing through a Drierite gas-drying unit (Sigma-Aldrich) before use. Tetrahydrofuran (THF) was dried over CaH_2 and distilled from $LiAlH_4$. The residual solvent was removed in vacuum below 1 Torr at 40 °C. All reactions, unless stated otherwise, were carried out under an inert atmosphere using anhydrous solvents.

*Synthesis of MD*n*−COOH, for* n = *0−3*. The synthesis of initial hydrophobic monodendrons was described in detail elsewhere.[22] Functionalized monodendrons have been synthesized as follows. To obtain MD0−COOH, a solution of 8.8 mmol of butyllithium in 3.51 mL of hexane (2.5 M solution) was added dropwise to a solution of MD0 (2.2 g, 8.8 mmol) in 70 mL THF, while the temperature was kept between −75 and −70 °C, and then the solution was stirred at −78 °C for 1 h. Next, 300 mL (13.2 mmol) of carbon dioxide was introduced for 1 min, keeping the temperature below −60 °C. The solution was stirred at −70 °C for 30 min. It was then poured into 100 mL of water, containing an equimolar amount of hydrochloric acid (13.2 mL of 1 M HCl). After vigorous shaking, three extractions with 100 mL of diethyl ether were carried out. The organic solution was dried over sodium sulfate. The solvent was evaporated in vacuum, and the residue was dried at 1 Torr to give 2.56 g of crude product in a reaction yield of 95% (according to ^{1}H NMR). The crude product was purified by recrystallization from a hexane/ethylacetate mixture (2:1) to give pure compound MD0−COOH (2.3 g, 89%), mp 120 °C (literature value of 112 °C).[23] IR ν (KBr): 1678 cm^{-1} (C═O). ^{1}H NMR (250 MHz, DMSO-CCl_4) δ: 0.88 (t, 3 H, J = 6.7 Hz), 1.24−1.40 (overlapped peaks, 6 H), 1.63 (m, 2 H, M = 5, J = 6.7 Hz), 2.78 (t, 2 H, J = 7.3 Hz), 6.74 (d, 1 H, J = 3.6 Hz), 7.11 (d, 1 H, J = 4.28 Hz), 7.14 (d, 1 H, J = 3.7 Hz), 7.56 (d, 1 H, J = 4.28 Hz), 12.80 (broadened signal, 1 H). ^{13}C NMR (125 MHz, $CDCl_3$) δ: 14.07, 22.56, 28.73, 30.21, 31.48, 31.52, 123.30, 125.24, 125.39, 129.55, 133.47, 135.91, 146.65, 147.90, 167.82. MS−EI (70 eV): m/z 294.0748 (M$^+$, requires 294.0744).

MD1−COOH was obtained as described for compound MD0−COOH using 1.00 g (1.40 mmol) of compound MD1, 0.93 mL of 1.6 M butyllithium solution in hexane (1.4 mmol), 48 mL (2.10 mmol) of carbon dioxide, and 30 mL of THF to give the crude product in a reaction yield of 98% (according to ^{1}H NMR). The crude product was purified by gradient column chromatography on silica gel (eluents: 1:3 toluene/hexane and ethyl acetate) to give pure compound MD1−COOH (0.79 g, 75%), mp 116 °C. IR ν (film): 1671 cm^{-1} (C═O). ^{1}H NMR (250 MHz, DMSO-CCl_4) δ: 0.88 (t, 6 H, J = 6.7 Hz), 0.93 (s, 3 H), 1.23−1.39 (overlapped peaks, 12 H), 1.64 (m, 4 H, M = 5, J = 6.7 Hz), 2.76 (t, 4 H, J = 7.3 Hz), 6.69 (d, 2 H, J = 3.7 Hz), 7.03 (d, 2 H, J = 3.7 Hz), 7.21 (d, 2 H, J = 3.7 Hz), 7.26 (d, 1 H, J = 3.7 Hz), 7.29 (d, 2 H, J = 3.7 Hz), 7.35 (d, 1 H, J = 3.7 Hz), 7.45 (d, 1 H, J = 3.7 Hz), 7.59 (d, 1 H, J = 3.7 Hz), 12.88 (broadened signal, 1 H). ^{13}C NMR (125 MHz, $CDCl_3$) δ: −0.28, 14.06, 22.55, 28.72,

(21) (a) *Dendrimers and Other Dendritic Polymers*; Fréchet, J. M. J., Tomalia, D. A., Eds.; Wiley: New York, 2001; p 647.(b) *Dendritic Molecules: Concepts, Syntheses, Perspectives*; Newkome, G. R., Moorefield, C. N., Vogtle, F., Eds.; VCH: Weinheim, Germany, 1996; p 261.(c) Peleshanko, S.; Tsukruk, V. V. *Prog. Polym. Sci*. **2008**, *33*, 523.

(22) Luponosov, Y. N.; Ponomarenko, S. A.; Surin, N. M.; Muzafarov, A. M. *Org. Lett*. **2008**, *10*, 2753.

(23) Kobmehl, G.; Labahn, B. *Z. Naturforsch., B: Chem. Sci*. **1996**, *58*, 286.

30.14, 31.50, 31.54, 124.04, 124.36, 124.67, 124.83, 126.86, 130.92, 132.38, 134.18, 135.80, 137.03, 137.86, 137.93, 142.88, 145.32, 145.36, 146.04, 167.49. ^{29}Si NMR (100 MHz, $CDCl_3$) δ: −25.12. Anal. Calcd for $C_{38}H_{42}O_2S_6Si$ (%): C, 60.76; H, 5.64; S, 25.61; Si, 3.74. Found: C, 61.01; H, 5.81; S, 25.33; Si, 3.69. MALDI−MS: m/z 750.1276 (M^+, requires 750.1269).

MD2−COOH was obtained as described for compound MD0−COOH using 1.11 g (0.7 mmol) of compound MD2, 0.41 mL of 1.6 M butyllithium solution in hexane (0.7 mmol), 23 mL (10 mmol) of carbon dioxide, and 35 mL of THF to give the crude product in a reaction yield of 99% (according to ^{1}H NMR). The crude product was purified by gradient column chromatography on silica gel (eluents: 1:3 toluene/hexane and ethyl acetate) to give pure compound MD2−COOH (0.95 g, 83%). IR ν (film): 1671 cm^{-1} (C═O). ^{1}H NMR (250 MHz, DMSO-CCl_4) δ: 0.87 (t, 12 H, J = 6.7 Hz), 0.91 (s, 6 H), 0.95 (s, 3 H), 1.23−1.36 (overlapped peaks, 24 H), 1.62 (m, 8 H, M = 5, J = 7.3 Hz), 2.75 (t, 8 H, J = 7.3 Hz), 6.68 (d, 4 H, J = 3.7 Hz), 7.02 (d, 4 H, J = 3.1 Hz), 7.20 (d, 4 H, J = 3.7 Hz), 7.26 (d, 1 H, J = 4.3 Hz), 7.28 (d, 4 H, J = 3.7 Hz), 7.31−7.41 (overlapped peaks, 9H), 7.47 (d, 1 H, J = 3.7 Hz), 7.58 (d, 1 H, J = 4.3 Hz), 12.86 (broadened signal, 1 H). ^{13}C NMR (125 MHz, $CDCl_3$) δ: −0.32, −0.18, 14.10, 22.58, 28.73, 30.16, 31.54, 31.56, 123.99, 124.36, 124.77, 124.84, 125.71, 125.78, 125.91, 132.82, 133.68, 134.27, 134.89, 134.78, 137.85, 138.00, 138.06, 143.79, 144.33, 145.20, 145.97. ^{29}Si NMR (100 MHz, $CDCl_3$) δ: −25.24, −24.92. Anal. Calcd for $C_{84}H_{90}O_2S_{14}Si_3$ (%): C, 60.60; H, 5.45; S, 26.96; Si, 5.06. Found: C, 60.63; H 5.49; S, 26.78; Si, 5.10. MALDI−MS: m/z 1665.2359 (M^+, requires 1665.2350).

MD3−COOH was obtained as described for compound MD0−COOH using 1.3 g (0.4 mmol) of compound MD3, 0.24 mL of 1.6 M butyllithium solution in hexane (0.4 mmol), 13 mL (0.6 mmol) of carbon dioxide, and 35 mL of THF to give the crude product in a reaction yield of 40% (according to ^{1}H NMR). The crude product was purified by gradient column chromatography on silica gel (eluents: 1:1 toluene/hexane and ethyl acetate) to give pure compound MD3−COOH (0.26 g, 20%). IR ν (film): 1671 cm^{-1} (C═O). ^{1}H NMR (250 MHz, DMSO-CCl_4) δ: 0.85 (t, 24 H, J = 6.7 Hz), 0.90 (s, 12 H), 0.93 (s, 9 H), 1.21−1.36 (overlapped peaks, 48 H), 1.61 (m, 16 H, M = 5, J = 7.3 Hz), 2.73 (t, 16 H, J = 7.3 Hz), 6.65 (d, 8 H, J = 3.7 Hz), 6.99 (d, 8 H, J = 3.1 Hz), 7.17 (d, 8 H, J = 3.1 Hz), 7.23 (d, 1 H, J = 3.7 Hz), 7.26 (d, 8 H, J = 3.7 Hz), 7.28−7.39 (overlapped peaks, 25 H), 7.44 (d, 1 H, J = 3.1 Hz), 7.57 (d, 1 H, J = 4.3 Hz). ^{13}C NMR (125, MHz, $CDCl_3$) δ: 0.26, 0.24, 0.19, 14.08, 22.55, 28.71, 30.14, 31.51, 31.53, 123.96, 124.33, 124.73, 124.81, 125.66, 125.70, 125.75, 125.79, 126.88, 132.82, 134.09, 134.26, 134.43, 134.72, 135.71, 137.83, 137.94, 138.05, 143.87, 144.14, 144.24, 145.15, 145.92. ^{29}Si NMR (100 MHz, $CDCl_3$) δ: −25.25, −25.09, −25.05. Anal. Calcd for $C_{176}H_{186}O_2S_{30}Si_7$ (%): C, 60.54; H, 5.37; S, 27.55; Si, 5.63. Found: C, 60.67; H, 5.57; S, 27.20; Si, 5.60. MALDI−MS: m/z 3599.3499 (M^+ + Ag, requires 3599.3490).

Substrates Preparation. Silicon substrates (1 × 2 cm) [100] (Semiconductor Processing) with a native silicon oxide layer with 1.6 nm thickness were cleaned with Piranha solution (3:1 concentrated sulfuric acid and hydrogen peroxide mixture, caution), abundantly rinsed with Nanopure water (18.2 MΩ cm), and dried with dry nitrogen stream in accordance with the usual procedure.[24] They served as hydrophilic substrates for film depositions, which were prepared either by spin coating from 1 mg/mL (1500 rpm, 30 s) chloroform solution or LB deposition. Quartz slides were prepared similarly: cut into 1 × 2 cm, rinsed with Nanopure water, sonicated at room temperature, and finally treated with Piranha solution. Similar to silicon substrates, quartz slides were last rinsed with Nanopure water and dried with dry nitrogen stream.

Methods. ^{1}H NMR spectra were recorded on a Bruker WP-250 SY spectrometer at 250 MHz using NMR-grade $CDCl_3$ or CCl_4−DMSO mixture as a solvent. ^{13}C NMR spectra were recorded on a Bruker DRX500 spectrometer at 125.76 MHz, and ^{29}Si NMR spectra were recorded on a Bruker DRX500 spectrometer at 99.36 MHz, using NMR-grade $CDCl_3$ as a solvent. Mass spectra (MALDI−MS) were recorded on a Bruker Daltonics Reflex-III mass spectroscope in the positive-ion regime using the reflection mode with a target voltage of 20 kV. 2,4, 9-Antracenetriol was used as a matrix. The samples were prepared by dissolution of the compounds under investigation in chloroform ($C = 10^{-4}-10^{-6}$ M) and mixed with a solution of the matrix (20 mg/mL) in chloroform in the ratio of 1:1. Mass spectra of MD0−COOH were recorded on Micromass M@ldi MALDI−TOF MS working in reflectron mode using dihydroxybenzoic acid (10 mg/mL in THF) as a matrix and CF_3COOAg (1 mg/mL THF) as an additive. Samples were prepared by dissolution of MD0−COOH in THF (1 mg/mL) and mixed with the matrix and additive in a 1:1:1 volume ratio. Mass spectra of MD0−COOH were recorded on Micromass M@ldi MALDI−TOF MS working in reflectron mode using dihydroxybenzoic acid (10 mg/mL in THF) as a matrix and CF_3COOAg (1 mg/mL THF) as an additive. Samples were prepared by dissolution of MD0−COOH in THF (1 mg/mL) and mixed with the matrix and additive in a 1:1:1 volume ratio.

The LB studies were conducted using a KSV2000 minitrough at room temperature, according to the usual procedure adapted in our lab.[25] A 40−120 μL solution (0.26−1.4 mg/mL) in chloroform (HPLC grade) was evenly dispersed in several droplets onto the surface of the Nanopure water. It was then left for 30 min to allow for the evaporation of the chloroform. Compression of the monolayers was conducted at a speed of 5 mm/min. The limiting cross-sectional area A_0 was determined by the steepest tangent rise in the surface pressure, which provided evidence of the formation of a condensed monolayer.[26]

Effective film thicknesses were obtained with a M-2000U spectroscopic ellipsometer (Woolam), equipped with WVASE32 analysis software. Images were obtained from a Dimension-3000 atomic force microscope (AFM) and a Leica DM4000 optical microscope. AFM topographical images were generated in the "light" tapping mode with low-amplitude set point (ratio within 0.90−1.0) to avoid monolayer damage.[27] The AFM cantilevers have spring constants in the range of 40−60 N/m. Scanning rates were chosen between 1.0 and 2.0 Hz, depending upon the scan area that ranges from 40 × 40 to 1 × 1 μm^2, in accordance with the procedures adapted in our lab.[28]

Fluorescence spectra were obtained with a RF-5301PC spectrofluorophotometer (Shimadzu). Quartz slides were used for UV/vis measurement with a UV-2450 spectrophotometer (Shimadzu). Emission spectra were registered in the wavelength range of 250−600 nm for excitation wavelengths in the range of 250−400 nm. In all cases, the optical density of the solutions used for the measurements of quantum yield did not exceed 0.05 in a 10 mm thick quartz cuvette. Density was measured according to the Archimedes method using a glycerine−water mixture as the fluid medium.

X-ray diffraction data were collected with an Alpha1-Philips analytical diffractometer. Analysis of X-ray diffraction data and the unit cell determination was performed with MDI Jade 7 X-ray diffraction software. TREOR90 algorithm was used for space group and peak assignments.[29] Molecular models were built with

(24) (a) Szunerits, S.; Boukherroub, R. *Langmuir* **2006**, *22*, 1660. (b) Sheller, N. B.; Petrash, S.; Foster, M. D.; Tsukruk, V. V. *Langmuir* **1998**, *14*, 4535.

(25) (a) Larson, K.; Vaknin, D.; Villavicencio, O.; McGrath, D. V.; Tsukruk, V. V. *J. Phys. Chem. B* **2002**, *106*, 7246. (b) Peleshanko, S.; Sidorenko, A.; Larson, K.; Villavicencio, O.; Ornatska, M.; McGrath, D. V.; Tsukruk, V. V. *Thin Solid Films* **2002**, *406*, 233.

(26) Ulman, A. *An Introduction to Ultrathin Organic Films: From Langmuir−Blodgett to Self-Assembly*; Academic Press: Boston, MA, 1991.

(27) Magonov, S. N.; Elings, V.; Whangbo, M. H. *Surf. Sci.* **1997**, *375*, L385.

(28) (a) Tsukruk, V. V.; Reneker, D. H. *Polymer* **1995**, *36*, 1791. (b) Tsukruk, V. V. *Rubber Chem. Technol.* **1997**, *70*, 430.

(29) Pecharsky, V. K.; Zavalij, P. Y. In Fundamentals of Powder Diffraction and Structural Characterization of Materials; Kluwer Academic Publishers: Norwell, MA, 2003.

Table 1. Properties of MD*n*−COOH and MD*n* Dendrimers

MD*n*	M_w	number of bithiophene fragments	ε (M^{-1} cm^{-1})	$\lambda_{abs\text{-}max,\ THF}$	$\lambda_{abs\ max,\ quartz}$[a]	$\lambda_{fl\text{-}max,\ THF}$
0	250	1	13000	308	315	375
1	707	3	58100	333	337	372/382
2	1621	7	142800	333	342	373/386
3	3448	15	350000	333	342	373/387

MD*n*−COOH	M_w	number of bithiophene fragments	ε (M^{-1} cm^{-1})	$\lambda_{abs\text{-}max,\ THF}$	$\lambda_{abs\text{-}max,\ quartz}$	$\lambda_{fl\text{-}max,\ THF}$
0	294	1	23500	342	332	406
1	751	3	59150	335	344	377/391
2	1665	7	151000	335	343	383/396
3	3492	15	295000	335	343	377/391

[a] The UV/vis measurement was obtained for spin-casted film from 1 mg/mL solution in $CHCl_3$ on a quartz slide.

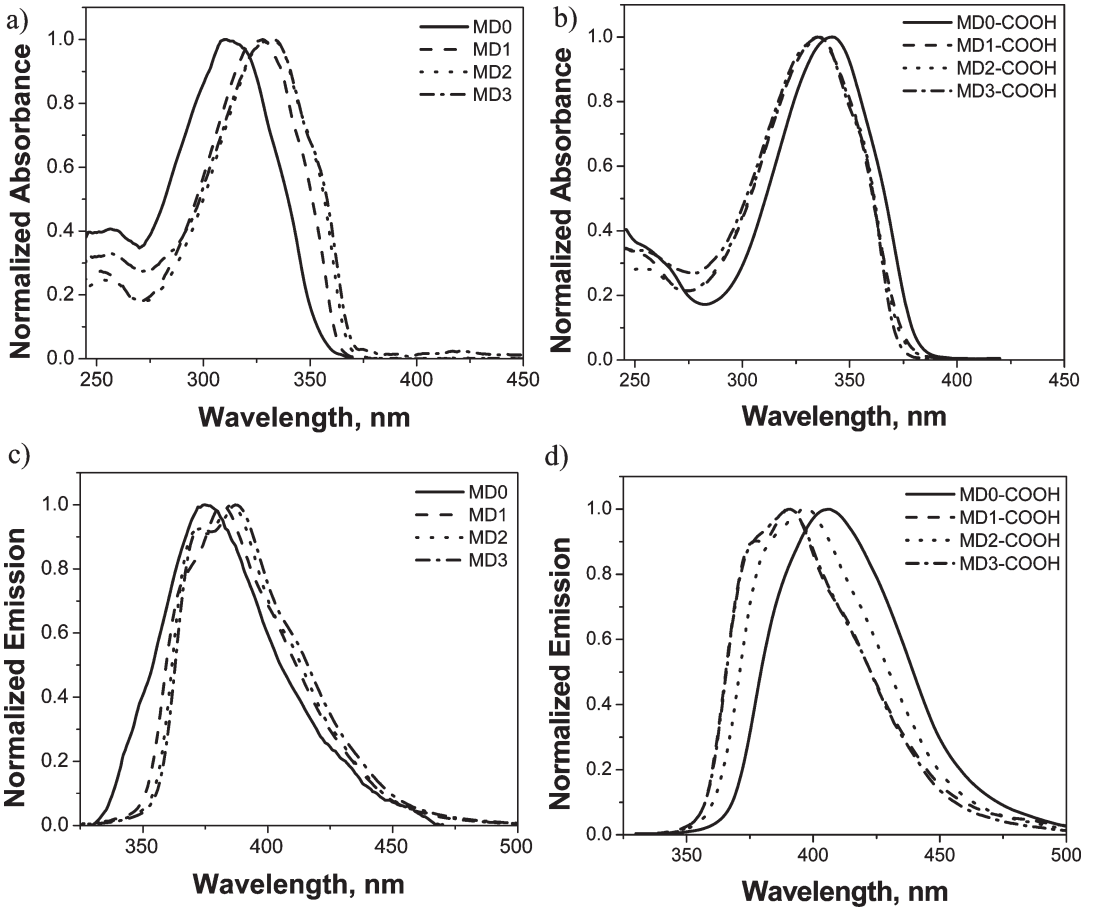

Figure 2. UV/vis spectra of a dilute solution of (a) MD*n* and (b) MD*n*−COOH in THF. Photo-emission spectra of a dilute solution of (c) MD*n* and (d) MD*n*−COOH.

Materials Studio 3.1 software. Force fields for energy minimizations were assigned using the PCFF method available in the Materials Studio Discover 3.1 package.

Results and Discussion

Photoluminescent Properties of Bithiophenesilane Monodendrons. The branched bithiophenesilane monodendrons studied here have molecular weights below 4000 Da (Table 1). They are composed of bithiophene fragments (from 1 to 15), which are linked together by silicon atoms. Both the branched dendritic architectures and the hexyl chains that are attached to the bithiophene peripheries make them well-soluble in common organic solvents. The molar extinction coefficients, ε, as measured from Beer−Lambert's law for a series of dilute concentrations of MD*n* in THF ($C < 5 \times 10^{-5}$ M) show the increase from 13 000 to 350 000 M^{-1} cm^{-1} (Table 1). For MD*n*−COOH, the values range from 23 500 and 295 000 M^{-1} cm^{-1}. Except for the highest generation, $n = 3$, these values are generally smaller for MD*n* than that for MD*n*−COOH. The greatest and lowest values are achieved for MD3 and MD0, respectively. The linear plot of absorbance versus concentration confirms that, at the given concentrations ($< 5 \times 10^{-5}$ M), these molecules are non-interacting (not shown).[30]

The measured molar extinction coefficients, ε, for monodendrons studied here are much larger than the ε for thiophene

(30) Chen, J.; Li, S.; Zhang, L.; Liu, B.; Han, Y.; Yang, G.; Li, Y. *J. Am. Chem. Soc.* **2005**, *127*, 2165.

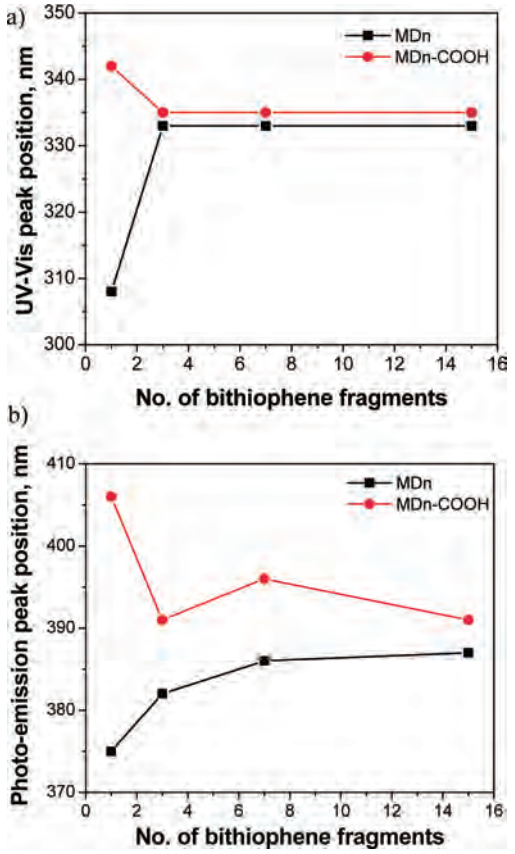

Figure 3. Plots of the (a) number of bithiophene fragments versus UV/vis peak position (nm) and (b) number of bithiophene fragments versus photo-emission peak position (nm) in dilute THF solution.

dendrimers having similar generations that were reported by Xia et al.[12c] For dendrimers having 3, 6, 7, 14, and 15 thiophene molecules directly linked at the α positions, reported values of ε are between 9700 and 56 400 M^{-1} cm^{-1}. These dendrimers have solubilizing hexyl chains at the periphery. Thus, the main difference between our systems and compounds from Xia et al. is that our dendrons are composed of bithiophene fragments that are isolated by silicon branching points that break conjugation. Another comparison can be made for phenyl-cored thiophene dendrimers, which also, because of conjugation, show a smaller value of ε for dendrimers that contain 12−32 thiophene molecules. The values of ε for these compounds ranged from 76 000 to 112 000 M^{-1} cm^{-1}.[34]

The presence of a focal COOH group in the monodendrons causes the absorption and fluorescence maxima to red shift with respect to MD*n* monodendrons, and the shift is most significant for the linear MD*n*−COOH compound (Figure 2). This is due to the electron-withdrawing nature of the carboxylic group,[31] as well as increased conjugation length. Dilute THF solution absorption maxima of MD*n* monodendrons, which corresponds to the $\pi-\pi^*$ electronic transition,[32] lie between 308 and 333 nm, whereas dilute THF solution absorption maxima of MD*n*−COOH monodendrons are between 335 and 342 nm. These values are smaller than those for a similar thiophene molecule, α-hexadecylterthiophene (C_{16}-3T), which absorbs at 366 nm. The red-shifted absorption maximum in C_{16}-3T is due to the increased conjugation length in the terthiophenes as compared to bithiophenes.[33] The alkyl substituent is electron-donating and, depending upon the position of the thiophene ring, can cause either a red or blue shift.[34] When placed at the α,ω position, the alkyl substituent leads to better coplanarity of the molecule and therefore causes a red shift. On the contrary, the alkyl substituent at the β position will induce a blue shift because of some torsion of the molecule along the long axis, as a result of steric interactions induced by the pendant alkyl group.

It is worth noting that the UV/vis maximum absorption for MD*n* monodendrons red shifts for $n = 1-3$ as compared to $n = 0$, but in the case of MD*n*−COOH, a blue shift is observed (panels a and b of Figure 2 and Figure 3a). The contrasting trends in the shift in peak position appear to be symmetrical. Red shift is usually observed for higher generation dendrimers because of increased intramolecular interactions, which is consistent with that observed for the MD*n* monodendrons. However, when the larger molecule experiences steric limitations that, in turn, causes the dendron fragments to twist out of plane, it leads to a slight decrease in conjugation. When this distortion occurs, a blue shift in the UV/vis maximum absorption spectrum is observed instead, which is seen for the amphiphilic MD*n*−COOH monodendrons.[35]

Photo-emission spectra in dilute THF solution were obtained for all samples using excitation wavelength that corresponds to their $\lambda_{abs\text{-}max}$ (panels c and d of Figure 2 and Figure 3b). In parallel with the trend in the UV/vis peak positions, the presence of a COOH-withdrawing group causes the $\lambda_{fl\text{-}max}$ to red shift in MD*n*−COOH with respect to MD*n* monodendrons. The photo-emission peak maximum occurs between 372 and 387 nm (violet) for MD*n* monodendrons and between 377 and 406 nm (violet−indigo) for MD*n*−COOH monodendrons (Table 1). The emission spectrum is typically a mirror image of the absorption spectrum. This is especially true when the electronic excitation does not greatly influence the nuclear geometry.[36]

In addition, multiple peaks were observed with increasing dendron generations. This is indicative of additional intramolecular energy transfer from higher band gap, which, in this case, is for isolated bithiophene molecules, to the lowest band gap for interacting bithiophene fragments within the single monodendron molecules having multiple fragments.[12c]

Bulk Structure and Properties. MD0−COOH is a pale-yellow solid powder, whereas its hydrophobic MD0 counterpart is a viscous liquid at room temperature. The rest of the monodendron samples exhibit waxy or oily appearance at room temperature that suggests amorphous structures. The pale-yellow powder exhibits fluorescence when observed under UV light, $\lambda_{exc} = 380$ nm (Figure 4a).

Differential scanning calorimetry (DSC) measurements on all monodendron samples revealed that only MD0−COOH and MD1−COOH show sharp endothermic transitions, which implies the presence of the crystalline state (see Figures S1 and S2 in the Supporting Information). Moreover, MD0−COOH shows two enantiotropic phase transitions during first and second heating curves at 121 °C with the enthalpy of 99 J/g and at 169 °C with the enthalpy of 5.6 J/g (see Figure S2b in the Supporting Information). However, upon cooling, the lower peak splits into

(31) Bourgeaux, M.; Skene, W. G. *J. Org. Chem.* **2007**, *72*, 8882.
(32) Qiu, Y. Q.; Xu, Y.; Zhu, D. B. *Synth. Met.* **1997**, *84*, 197.
(33) Murphy, A. R.; Chang, P. C.; VanDyke, P.; Liu, J.; Frechet, J. M. J.; Subramian, V.; DeLongChamp, D. M.; Sambasivan, S.; Fischer, D. A.; Lin, E. K. *Chem. Mater.* **2005**, *17*, 6033.
(34) Yassar, A.; Horowitz, G.; Valat, P.; Wintgens, V.; Hmyene, M.; Deloffre, F.; Srivastava, P.; Lang, P.; Garnier, F. *J. Phys. Chem.* **1995**, *99*, 9155.
(35) Mitchell, W. J.; Kopidakis, N.; Rumbles, G.; Ginley, D. S.; Shaheen, S. E. *J. Mater. Chem.* **2005**, *15*, 4518.
(36) Lakowicz, J. R. *Principles of Fluorescence Spectroscopy*, 3rd ed.; Springer Science: Singapore, 2006.

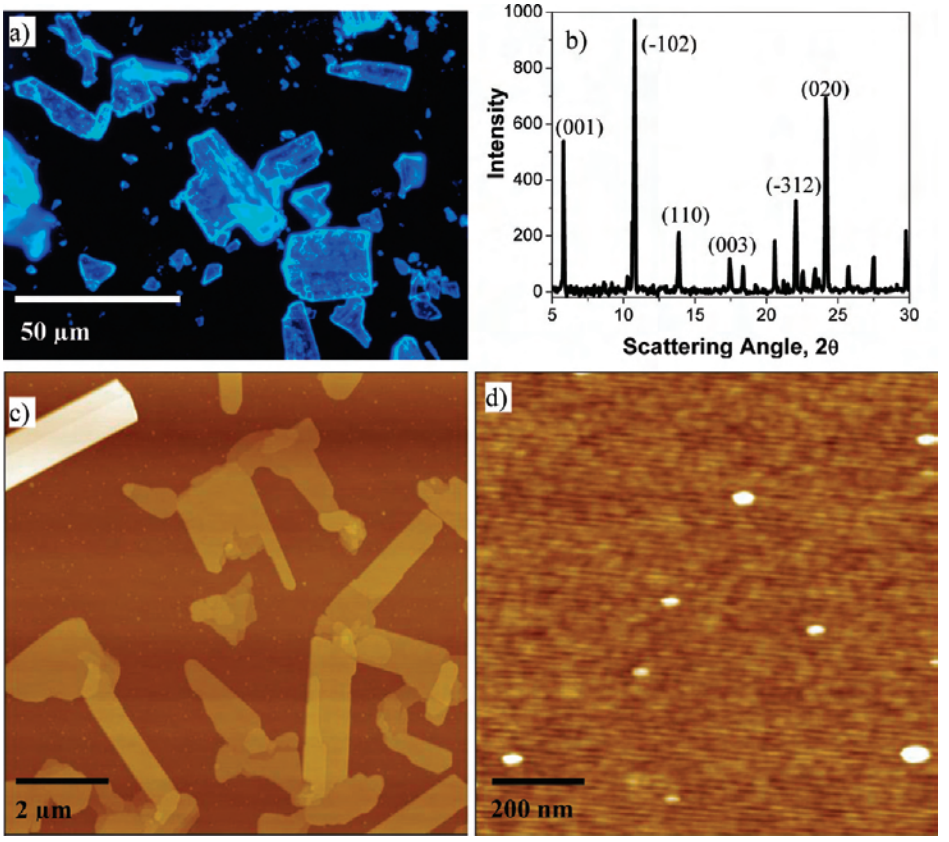

Figure 4. (a) Fluorescence image of MD0−COOH and (b) X-ray diffraction pattern of MD0−COOH in the bulk state. AFM height image of spin-coated samples from 1 mg/mL chloroform solution (Z = 200 nm): (c) MD0−COOH and (d) MD0.

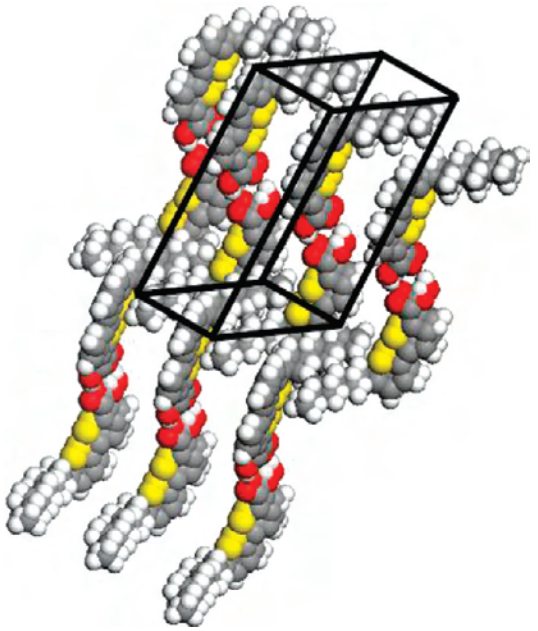

Figure 5. Proposed solid-state molecular arrangement of MD0−COOH in a head−head configuration within a monoclinic crystal system.

two sharp transitions, indicating recrystallization or the presence of a mesophase. The first peak at 102 °C possesses the enthalpy of 45 J/g, and a second peak at 89 °C has the enthalpy of 52 J/g. Optical polarizing microscopy upon cooling in the temperature interval of 170−103 °C showed schlieren texture, characteristic of a nematic mesophase, and in the interval of 102−60 °C showed a less familiar bright texture, which probably, corresponds to an ordered smectic mesophase (see Figure S3 in the Supporting Information). Further cooling led to a dark crystal texture. For MD1−COOH, a phase transition occurs at 118 °C with the enthalpy of 52 J/g during the first heating scan only. The second scan for this substance shows only the glass transition in the region of −6 °C, indicating its amorphous state.

Indeed, sharp peaks with no discernible broad halo peaks are obtained from X-ray diffraction measurements, confirming the high crystallinity of MD0−COOH sample, as concluded from DSC (Figure 4b). Despite evidence of crystallinity from DSC measurements, X-ray diffraction of MD1−COOH did not yield sufficient crystalline peaks for a meaningful interpretation (not shown). Exhaustive indexing of MD0−COOH yields a primitive monoclinic crystal system with $P2_1$ (4) being the most likely space group, with the c dimension closely corresponding the length of a single MD0−COOH molecule, 1.7 nm (Figure 5). The corresponding unit cell parameters are a = 1.4 nm, b = 0.7 nm, c = 1.7 nm, $\alpha = 90°$, $\beta = 114.5°$, and $\gamma = 90°$, and unit cell volume is 1596 nm^3. Considering the measured density of 1.12 ± 0.01 g/cm^3, we can conclude the presence of four molecules per unit cell, which yields the packing coefficient of 0.75.[37] Head−head packing configuration suggested here for MD0−COOH can be stabilized by hydrogen bonding between COOH groups and hydrophobic interactions between alkyl chains (Figure 5).

The packing for linear biothiphene molecules suggested here closely resembles that reported for 4-[[4-(alkoxy)phenyl]azo]benzoic acid.[38] Both compounds contain a aromatic rigid backbone that is capable of forming either a herringbone or a π-stack

(37) Dunitz, J. D. *X-ray Analysis and the Structure of Organic Molecules*; Verlag Helvatica Chimica Acta: Weinheim, Germany, 1995.
(38) Sano, M.; Sasaki, D. Y.; Isayama, M.; Kunitake, T. *Langmuir* **1992**, *8*, 1893.

Table 2. Characteristics of Spin-Coated *n*th Generation Carboxyl-Terminated, MD*n*−COOH, and Fully Hydrophobic Bithiophenesilane Monodendrons, MD*n*, with $n = 0-, 1, 2,$ and 3

sample names	domain heights, H (nm)	domain surface coverage, A_c	effective film thickness, t (nm)	calculated monolayer height (nm)[a]
MD0−COOH	14	0.4	6.5	0.9
MD1−COOH	60	0.08	7.2	2.4
MD2−COOH	55	0.11	8.0	2.0
MD3−COOH	15	0.25	7.2	3.5
MD0	0	0	5.5	5.5
MD1	325	0.03	10.6	0.9
MD2	110	0.09	10.5	0.6
MD3	4.5	0.6	7.2	4.3

[a] This value is calculated as $H - (A_c t)$.

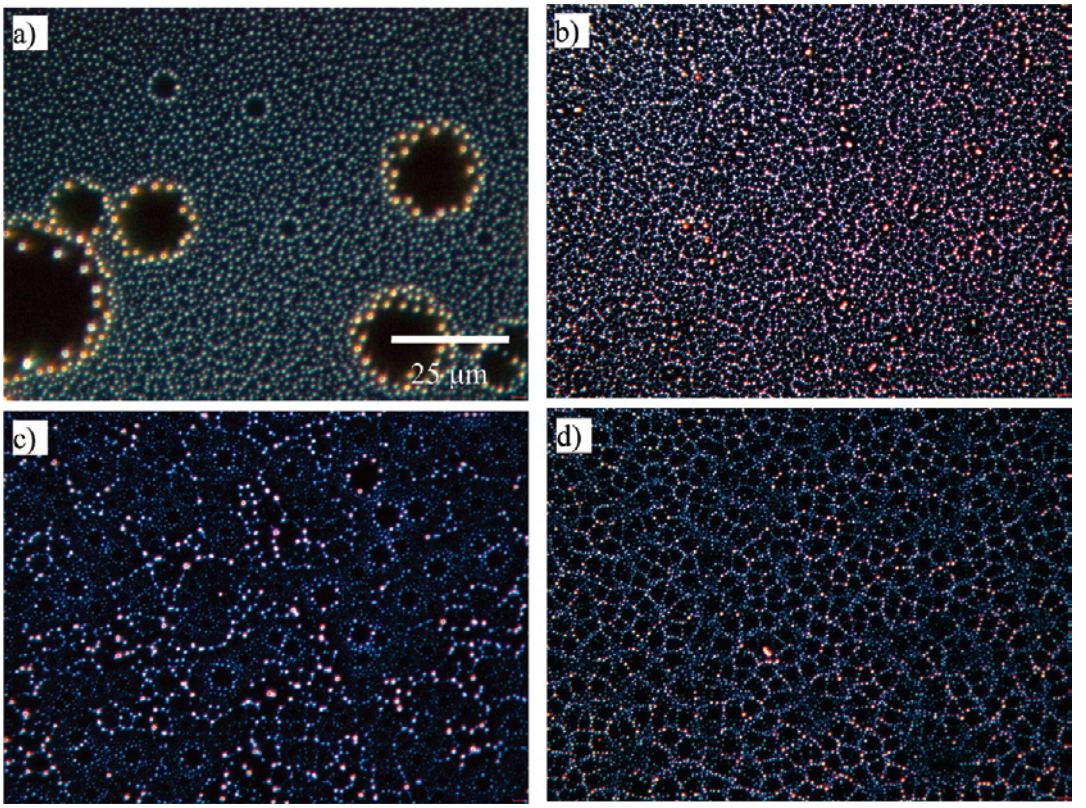

Figure 6. Representative dark-field optical images of spin-cast *n*th generation carboxyl-terminated, MD1 and MD2, (a and c, respectively) and fully hydrophobic bithiophenesilane monodendrons, MD1−COOH and MD2−COOH (b and d, respectively). All images are of the same magnification.

structure with a hydrophobic alkyl chain on one end and a hydrophilic carboxylic group on the other end. A single-crystal X-ray diffraction study of 4-[[4-(alkoxy)phenyl]azo]benzoic acids revealed a low symmetry space group, P-1, belonging to the triclinic crystal system.

Surface Films from Monodendrons. The solution of monodendrons spin cast onto hydrophilic silicon substrates formed aggregates with facets for MD0−COOH, whereas MD0 formed a uniform film (compare panels c and d of Figure 4). All other compounds, i.e., the amphiphilic MD*n*−COOH and fully hydrophobic MD*n* monodendrons, showed significant dewetting (Figure 6).

Closer examination of these surface films suggests that the multilayered structures is composed of globular aggregates residing on an underlying monolayer (Figure 7). The thickness of the underlying monolayer, also verified from AFM scratch test, was within 0.6−5.5 nm (Table 2). These values are within the height of a single monodendron molecule estimated from the molecular model (Figure 8). The effective thickness of these films ranged between 5 and 11 nm as measured with ellipsometry (Table 2). AFM height images enabled direct measurement of the heights of the globular aggregates, which ranged from 4.5 to 325 nm, indicating the formation of bulk aggregates (Table 2).

The dewetting of the upper layer into globular aggregates can be associated with aggregation, which minimizes the total surface energy that implies weak intermolecular interactions between the successive layers. It is well-known that films with thickness less than 100 nm might undergo three different stages of dewetting instabilities on solid substrates: (1) cylindrical holes are formed sporadically throughout a smooth film; (2) the holes grow into rims, which eventually turn into "cellular" structures; (3) and finally they turn into droplets.[39] Apparently, the final stage of dewetting is observed for thin surface films from our monodendrons. It is worth noting

(39) (a) Reiter, G. *Phys. Rev. Lett.* **1992**, *68*, 75. (b) Zhao, J.; Jiang, S.; Wang, Q.; Liu, X.; Ji, X.; Jiang, B. *Appl. Surf. Sci.* **2004**, *236*, 131.

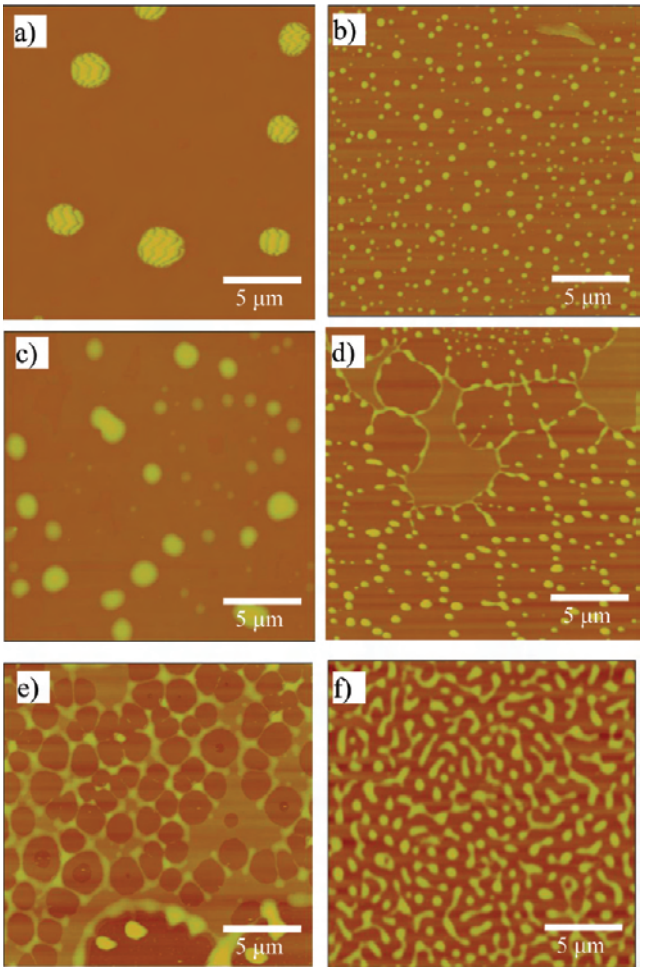

Figure 7. Representative AFM topography of spin-cast (a and b) MD1 and MD1−COOH, (c and d) MD2 and MD2−COOH, and (e and f) MD3 and MD3−COOH. The *Z* scale is 300 nm.

that similar surface behavior was previously reported for other dendritic thiophene derivatives.[12c]

The spin-coated film of 0th generation MD0−COOH monodendron showed a blue shift (Figure 9). In contrast, the UV/vis absorption spectra of the surface films of other MD*n*−COOH (n = 1−3) monodendrons showed red-shifted maxima compared to the dilute solution, indicating significant molecular aggregation, as suggested from AFM studies (Table 1). The most extreme red shift is observed for MD1, indicating enhanced intermolecular interactions and improved conjugation.[40] Moreover, intermolecular interactions caused the peak widths of the absorption spectra to widen, and additional shoulder peaks are also observed (Figure 9). As a result of significant intermolecular interactions and quenching, a relatively weak photoluminescence was obtained for these films with photoluminescence for MD*n*−COOH series, following the same trend as MD*n* series.

Generally, this surface behavior corresponds to that discussed in a theoretical study on amphiphilic α,ω-substituted oligothiophenes on hydrophilic and hydrophobic substrates, which concluded that the overall surface morphology is determined by the balance of molecule−substrate and molecule−molecule interactions.[41] Three possible scenarios were considered: (1) comparable molecule−molecule and molecule−substrate interactions; (2) the molecule−molecule interaction is much stronger than the molecule−substrate interaction; and (3) the molecule−substrate interaction is much stronger than the molecule−molecule interaction. In the first case, a uniform layered growth should be observed. In the second case, 3D layered island growth is observed. In the third case, the first layer of molecules will lie parallel to the substrate, but the subsequent deposition should result in aggregation. Our results clearly show that the MD0−COOH monodendrons studied here fall under the second category. The much stronger molecule−molecule interactions led to their crystallization, resulting in a 3D aggregation. The higher generation monodendrons fall under the third category; i.e., the first layer of molecules forms a uniform monolayer spread evenly over the solid substrate, but there is no sufficient intermolecular energy to build the next uniform molecular layer. As a result, the excess molecules rather form globular aggregates, thus preventing the formation of thin (from tens to hundreds of nanometers in thickness) uniform surface layers. Apparently, a similar situation is realized if surface films of comparable thickness are fabricated with sequential layered deposition, as will be discussed in the next section.

Langmuir Monolayers from COOH-Containing Monodendrons. The isotherm of the fully hydrophobic MD*n* molecules did not show an increase in surface pressure when compressed (not shown). Only the carboxyl-terminated monodendrons formed a stable Langmuir monolayer at the air−water interface because of the presence of the highly polar focal group (Figure 10a). The MD*n*−COOH series for n = 1−3 show the conventional Langmuir behavior that is characteristic for balanced amphiphilic compounds.[42] The Langmuir isotherms of MD*n*−COOH monodendrons for n = 1−3 show an extended plateau and collapsed at an intermediate surface pressure, between 10 and 20 mN/m (Figure 10a). The cusp on the isotherm represents the transition from a strong elastic response to a viscous response.[43] The overall shape of the Langmuir isotherms was similar to that reported for rigid third generation poly(benzyl ether) monodendrons with oligo(ethylene glycol) tails.[44] The derived areas per molecule from their Langmuir isotherms for MD*n*−COOH monodendrons for n = 1−3 are in the same range with photochromic amphiphilic azobenzene monodendrons, with carboxylic terminal group having the same number of alkyl tails (1, 2, 4, and 8).[45] The surface area per molecule ranged from 0.24 to 1.50 nm^2 for these molecules.

The area per molecule derived from the tangent line of the slope that lead to the collapsed point corresponds to the limiting molecular area in the condensed state.[26] It increases from 0.02 to 0.94 nm^2 from 0th to 3rd generation monodendrons (Figure 10a and Table 3). The difference in the surface area per molecule is significant between the first and second generation but is smaller between the second and third generation, i.e., 0.28 versus 0.06 nm^2. The area per molecule for MD0−COOH is inconsistent with even the most extreme scenario, where the thiophene rings adopt an edge-on orientation on the water surface, which should occupy a minimum area of about 0.2 nm^2.[32] Thus, we concluded that, for this compound, the unrealistic limiting area per molecule indicates strong aggregation behavior with the formation of bulky aggregates (Figure 10a).

(40) Dingemans, T. J.; Bacher, A.; Thelakkat, M.; Pedersen, L. G.; Samulski, E. T.; Schmidt, H.-W. *Synth. Met.* **1999**, *105*, 171.
(41) Surin, M.; Leclere, P.; De Feyter, S.; Abdel-Mottaleb, M. M. S.; De Schryver, F. C.; Henze, O.; Feast, W. J.; Lazzaroni, R. *J. Phys. Chem. B* **2006**, *110*, 7898.
(42) Dos Santos, C. G.; de Melo, C. P.; Souto Maior, R. *Synth. Met.* **1995**, *71*, 2083.
(43) Deng, J.; Hottle, J. R.; Polidan, J. T.; Kim, H.-J.; Farmer-Creely, C. E.; Viers, B. D.; Esker, A. R. *Langmuir* **2004**, *20*, 109.
(44) Kampf, J. P.; Frank, C. W.; Malmström, E. E.; Hawker, C. J. *Langmuir* **1999**, *15*, 227.
(45) Genson, K. L.; Holzmuller, J.; Villancencio, O. F.; McGrath, D. V.; Vaknin, D.; Tsukruk, V. V. *J. Phys. Chem. B* **2005**, *109*, 20393.

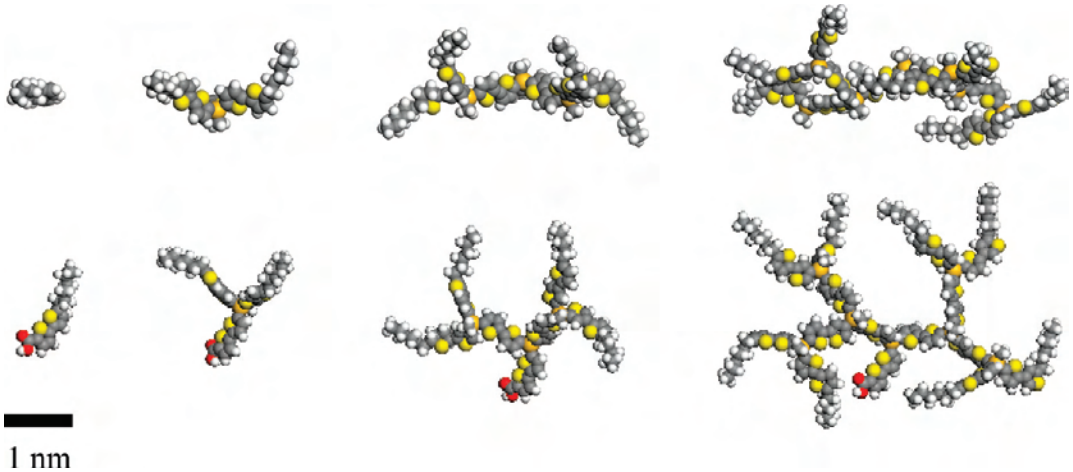

Figure 8. Molecular models of MDn−COOH molecules, for n = 0−3: (top row) top view and (bottom row) side view.

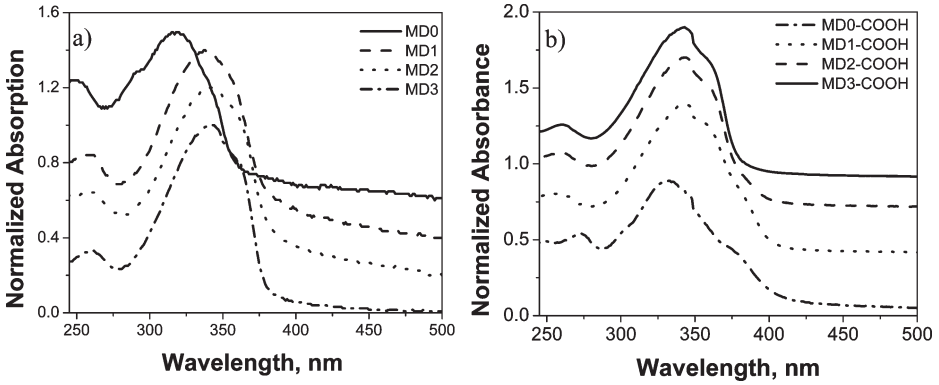

Figure 9. UV/vis absorption spectra of spin-cast films: (a) MDn and (b) MDn−COOH, with n = 0−3. Graphs have been offset for clarity.

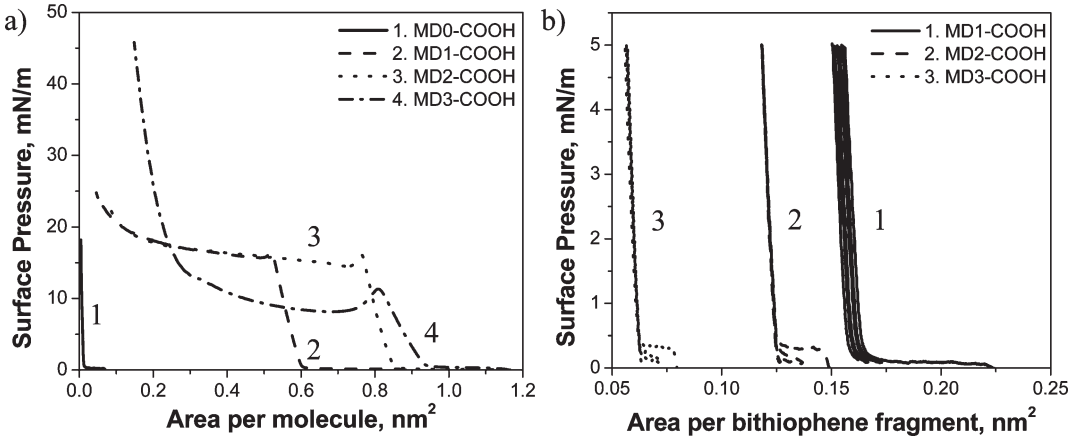

Figure 10. (a) Langmuir isotherms of carboxyl-terminated MDn−COOH monodendrons with n = 0−3. (b) Reversibility of Langmuir isotherms for MDn−COOH with n = 1−3.

Molecular modeling of monodendrons in possible conformations with branches predominantly oriented vertically and minimized energy predicts a slightly larger area per molecule, from 0.39 to 2.3 nm^2 than that observed experimentally (Figure 8 and Table 3). This suggests that the molecules are in a more condensed state within a dense Langmuir monolayer than that presented in Figure 8. The increasing limiting surface area per molecule with increasing monodendron generation contradicts that estimated from the corresponding molecular models (Table 3). The deviation from linearity in the area per molecule may be explained by the increasing role of intramolecular interaction with increasing monodendron generation, because of crowding of peripheral groups. This can be seen from the plot of surface pressure versus area per bithiophene fragments for the compression−decompression cycle, which reveals that the value of per bithiophene fragment area per molecule indeed decreases with increasing monodendron generation (Figure 10b). The graph also shows that within a constant surface pressure P = 5 mN/m for MDn−COOH, n = 1−3, the isotherms are nearly reversible, indicating that the monolayers are compressible and capable of recovery during decompression because of the presence of the silicon spacer atoms.

Table 3. Langmuir Isotherms Data for *n*th Generation Carboxyl-Terminated, MD*n*−COOH, with $n = 1$, 2, and 3

sample names	area per molecule (nm^2)	estimated area per molecule (nm^2)	monolayer thickness (nm) $P = 0.5$ mN/m	$P = 5$ mN/m	$P = 20$ mN/m
MD1−COOH	0.6	0.7	1.9	1.8	5.6
MD2−COOH	0.88	1.4	1.5	3.1	9.6
MD3−COOH	0.94	2.3	2.9	3.4	12.9

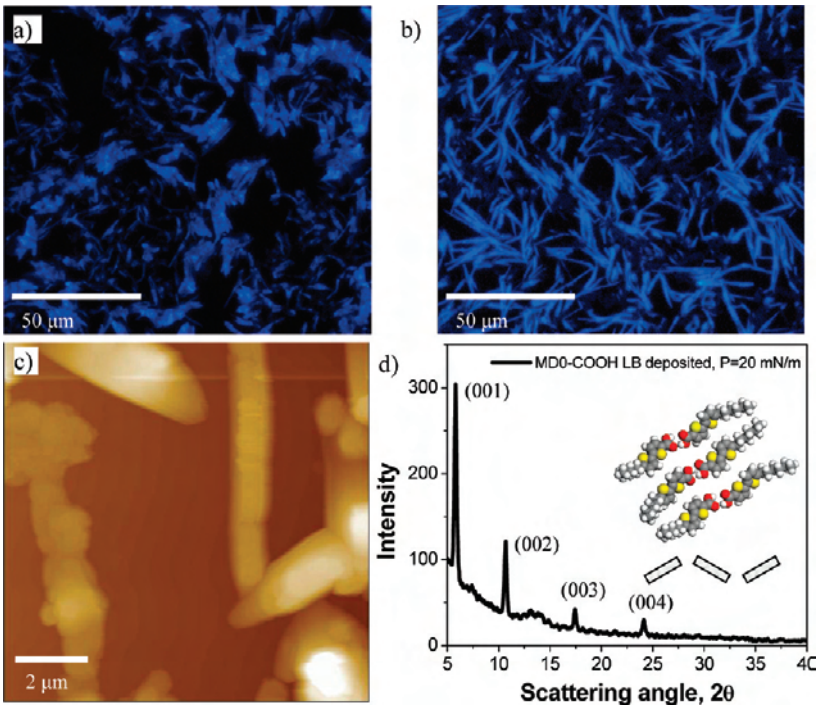

Figure 11. Fluorescence images of LB-deposited MD0−COOH monodendron at (a) $P = 0.5$ mN/m and (b) $P = 20$ mN/m ($\lambda_{exc} = 360$ nm). (c) AFM topographical image of b, $z = 200$ nm. (d) X-ray diffraction of MD0−COOH LB film at $P = 20$ mN/m. The inset is the proposed lamella arrangement of MD0−COOH molecules.

Surface Morphologies and Optical Properties of Langmuir Monolayers. The transfer ratio onto a silicon substrate for MD0−COOH monolayers was low (0.2−0.3), indicating the absence of uniform monolayers.[46] Optical microscopy confirmed that MD0−COOH formed 3D aggregates even at very low surface pressure, $P = 0.5$ mN/m (Figure 11a). The height of these aggregates determined from AFM images was about 60 nm, indicating their multilayer nature (Figure 11c). The aggregates formed sporadically, wherever nucleation sites happen, but they typically initiate along the edges of the LB trough. Upon compression, the number of nucleation sites increased; hence, denser aggregates are formed. At high surface pressure, high aspect ratio needle-like aggregates have been seen in optical and AFM images (Figure 11b). For high-concentration MD0−COOH solution (2.3 mg/mL, instead of 0.5 mg/mL), these aggregates formed as soon as the chloroform evaporated. In comparison to the crystals seen in spin-casted film, the majority of these crystals possess one-dimensional shape (compare Figure 4c to Figure 11b).

The X-ray diffraction peaks for these MD0−COOH aggregates occurred at $2\theta = 5.8°$, 10.7°, 17.4°, and 24.1° (Figure 11d). They correspond to the primary spacing of 15.2 Å and higher orders at 8.2, 5.01, and 3.7 Å, respectively. These spacings follow closely to the (00*l*) indexing from a layered packing with 1.5 nm thickness, which is very close to but slightly lower than the length of the extended molecules, indicating either tilting or partial interdigitation of molecules. Indeed, it has been demonstrated on many occasions that the rod-like molecules with alkyl tails tend to form layered structures with the alkyl tails, which can either form interdigitated packing or skewed packing in the *c* direction.[25,47,48]

The blue shift in the maximum UV/vis absorption spectrum was observed for the needle crystals from 342 nm in THF solution to 335 nm (Figure 12a). This shift suggests that the thiophene molecules in the (a, b) plane are arranged into a herringbone structure rather than a direct $\pi-\pi$-stack arrangement of backbones (inset in Figure 11d).[49,50] The intensity of the main peak increases and the intensity of the secondary peak at 270 nm decreases, indicating the dominance of bithiophene absorption in a solid monolayer state. A theoretical study on thiophene dimer interactions by Tsuzuki et al. concluded that, for unsubstituted and α-substituted thiophenes, herringbone arrangement is always

(46) Li, B.; Marand, H.; Esker, A. R. *J. Polym. Sci., Part B: Polym. Phys.* **2007**, *45*, 3300.

(47) (a) Curtis, M. D.; Cao, J.; Kampf, J. W. *J. Am. Chem. Soc.* **2004**, *126*, 4318. (b) Collard, D. M.; Stoakes, M. S *Chem. Mater.* **1994**, *6*, 850.

(48) (a) Sidorenko, A.; Houphouet-Boigney, C.; Villavicencio, O.; Hashemzadeh, M. McGrath, D. V.; Tsukruk, V. V. *Langmuir* **2000**, *16*, 10569. (b) Tsukruk, V. V.; Luzinov, I.; Larson, K. *J. Mater. Sci. Lett.* **2001**, *20*, 873.

(49) Zhang, X.; Johnson, J. P.; Kampf, J. W.; Matzger, A. J. *Chem. Mater.* **2006**, *18*, 3470.

(50) Yamamoto, T.; Komarudin, D.; Arai, M.; Lee, B.-L.; Saganuma, H.; Asakawa, N.; Inoue, Y.; Kubota, K.; Sasaki, S.; Fukuda, T.; Matsuda, H. *J. Am. Chem. Soc.* **1998**, *120*, 2047.

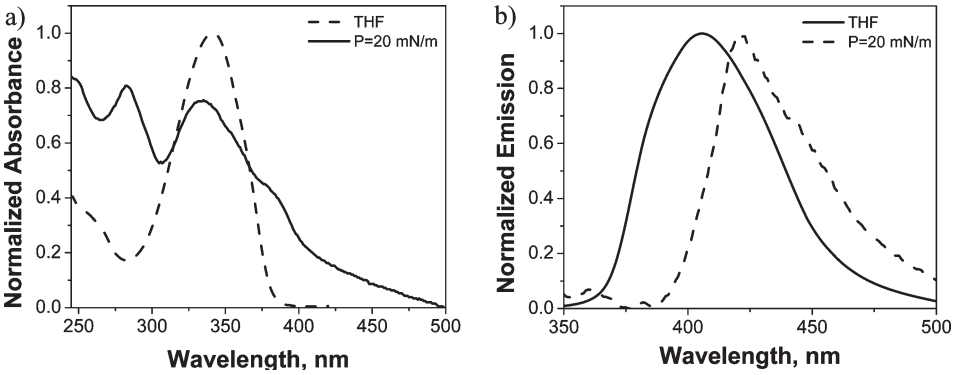

Figure 12. Spectra of the LB film of MD0−COOH at $P = 20$ mN/m and in dilute THF solution: (a) UV/vis and (b) fluorescence.

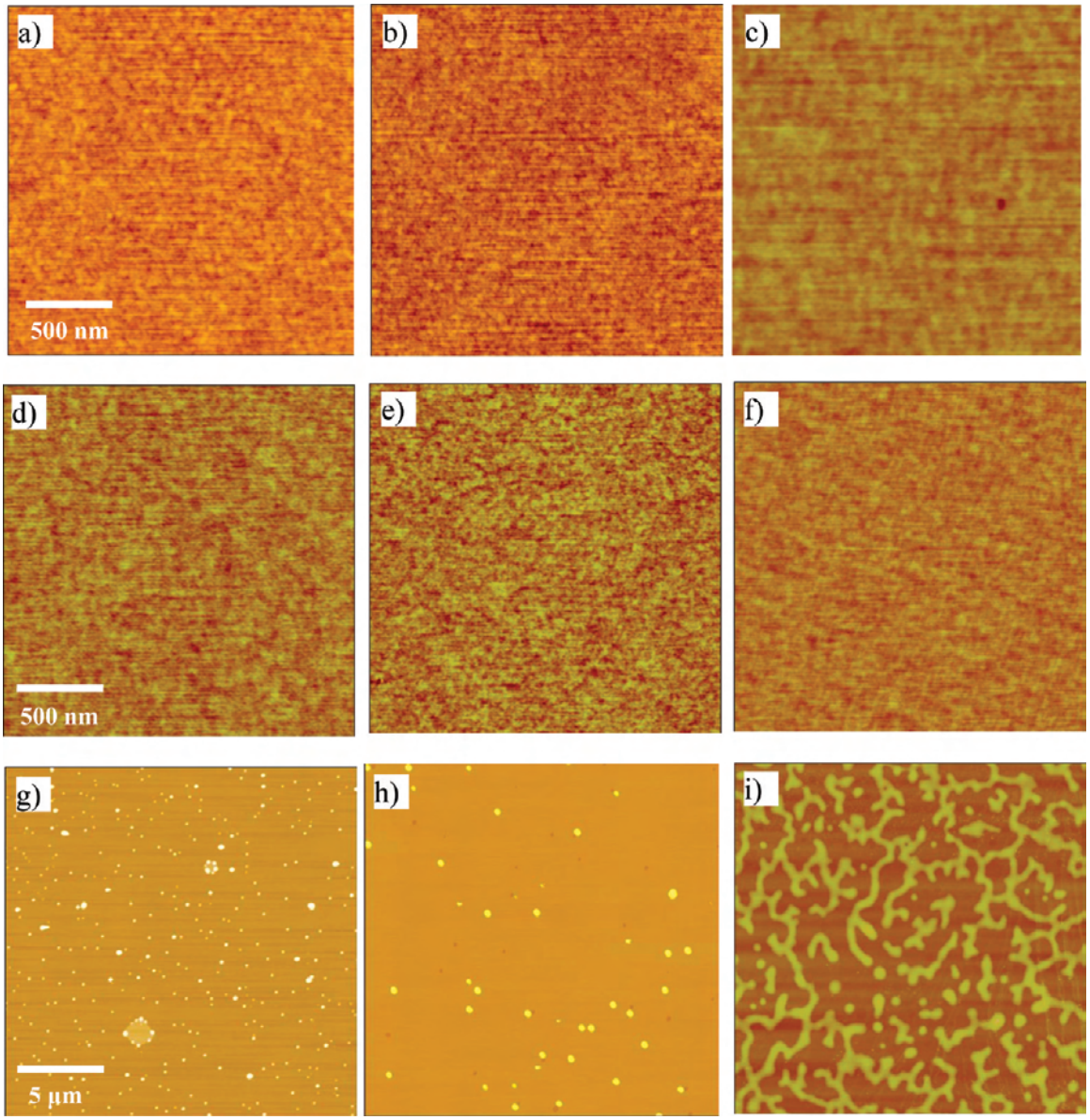

Figure 13. (a−i) LB monolayer of (a, d, and g) MD1−COOH (b, e, and h) MD2−COOH, and (c, f, and i) MD3−COOH bithiophenesilanes at different surface pressures, $P = 0.5$ mN/m (a−c), 5 mN/m (d−f), and 20 mN/m (g−i). The Z scale is 5 nm for a−f and 100 nm for g−i.

preferred over $\pi-\pi$ stacking because of much larger interaction energy between perpendicular thiophene dimers than parallel thiophene dimers.[51] Moreover, $\pi-\pi$ stacking is preferred for the β substituent because it destabilizes perpendicular dimers. Therefore, the proposed molecular arrangement for the α-substituted MD0−COOH molecules derived from X-ray, UV/vis, and photo-emission data is depicted in the inset of Figure 11d. It shows a lamellar arrangement, where the thiophene molecules are

(51) Tsuzuki, S.; Honda, K.; Azumi, R. *J. Am. Chem. Soc.* **2002**, *124*, 12200.

Table 4. UV/Vis for LB-Deposited MD*n*−COOH Monolayers, for $n = 1-3$, at Various Surface Pressures

	$P = 0.5$ mN/m		$P = 5$ mN/m		$P = 20$ mN/m		
sample names	λ_{max} (nm)	absorbance	λ_{max} (nm)	absorbance	λ_{max} (nm)	absorbance	in THF solution
MD1−COOH	339	0.02	339	0.04	352	0.13	335
MD2−COOH	341	0.05	341	0.05	342	0.37	335
MD3−COOH	342	0.11	342	0.101	344	0.30	335

non-coplanar. Similar to its bulk structure, both the presence of a crystallizable alkyl chain and hydrogen bonding between the carboxylic groups on the other end of the bithiophene molecules could promote alternating hydrophilic/hydrophobic packing.

Fluorescence measurement for these crystals shows that the emission peak red shifts in the solid state with respect to the dilute THF solution case, i.e., 421 nm in the solid state versus 406 nm in a dilute THF solution (Figure 12b). Additionally, the emission peak is narrower in the solid state and is accompanied with the appearance of a shoulder at 443 nm. The red shift of the emission maximum may indicate that the molecules are distorted in the solid state to accommodate planar lamellar structure. A second absorption peak is obviously red-shifted in the solid state at 283 nm. The more intense absorption peak corresponds to the absorption peak because of bithiophene units, and the less intense absorption peak corresponds to a single thiophene unit. For the single thiophene unit, the absorption peak does not depend upon the solvent used and occurs at 238 nm.[22] The red shift corroborates with the increased planarization of the bithiophene unit that facilitates energy transfer.

Unlike linear molecule (0th generation), all branched COOH-containing molecules formed uniform Langmuir monolayers on solid substrates (Figure 13). Representative surface morphologies of Langmuir monolayers for MD*n*−COOH ($n = 1-3$) deposited at $P = 0.5$, 5, and 20 mN/m showed similar trends over the range of surface pressures. The highest surface pressure, $P = 20$ mN/m, represents the surface morphologies following the cusp transition for MD1−MD3−COOH molecules. At a low surface pressure, $P = 0.5$ mN/m, very smooth and uniform monolayers were obtained with root-mean-square (rms) surface roughness of about 0.15 nm^2 within a 1×1 μm^2 area. The thickness of these monolayers is close to the height of a single MD*n*−COOH molecule (between 1.5 and 2.9 nm) (Table 3 and Figure 8). Upon further compression to $P = 5$ mN/m, the monolayer thickness increased slightly, up to 3.4 nm, which can be attributed to the increasing molecular density and further vertical alignment of thiophene branches. Finally, at $P = 20$ mN/m (above the transition on the isotherm), it became clear that we observe the onset of the formation of the globular aggregates as a result of the precollapse of the monolayers with a significant increase in rms surface roughness to approximately 10 nm over a 1×1 μm^2 area (Figures 10a and 13).

UV/vis spectroscopy allowed us to follow and confirm changes in molecular packing discussed above (photoluminescence intensity was too weak to be unambiguously recorded). Indeed, UV/vis spectra of MD*n*−COOH molecules deposited at several representative surface pressures, $P = 0.5$, 5, and 20 mN/m, showed a systematic increase in the absorbance intensity (up to 7-fold for the highest pressure), indicating the densification of the monolayer packing. As a result of the densification, the UV/vis absorption peak of the monolayer LB film is more red-shift than the spin-coated film (compare Table 1 to Table 4). The densification of the monolayer packing is confirmed from the increasing monolayer thickness and decreasing surface area available per molecules (Figure 14 and Table 4), as well as the shift in the UV/vis absorbance peak, as observed with an increasing surface

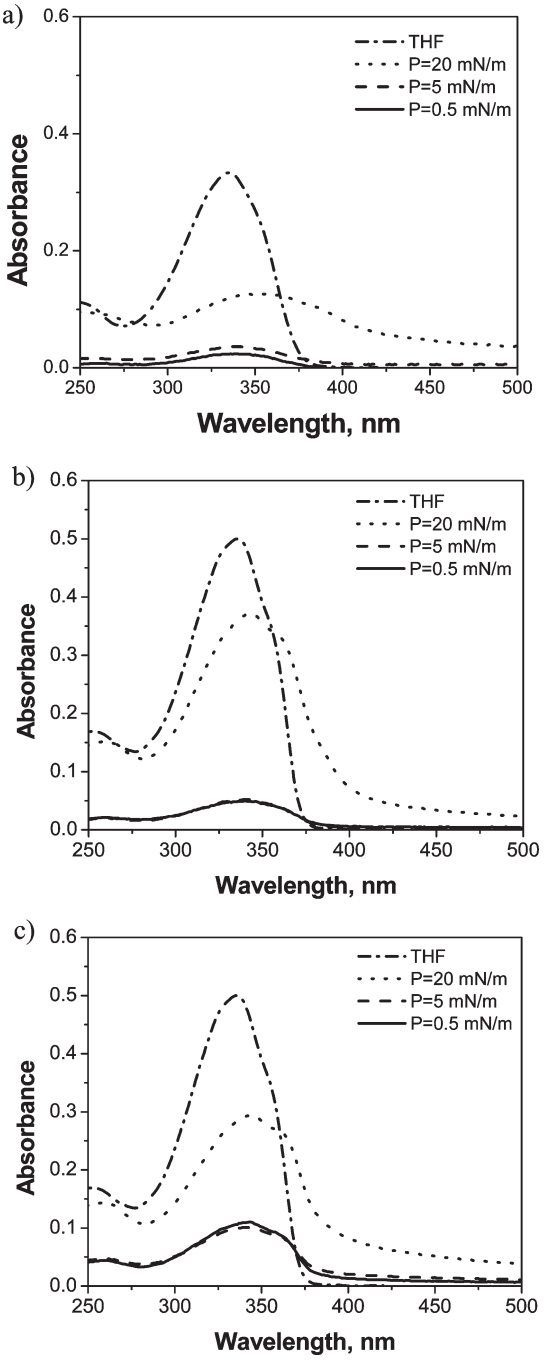

Figure 14. (a−c) UV/vis absorption spectra of MD*n*−COOH for $n = 1-3$, comparing dilute THF solution with LB-deposited films.

pressure (Figure 14). In all cases, the UV/vis absorbance peak for all generations at the lowest and medium surface pressure is significantly red-shifted as compared to isolated molecules in solution from 335 to 339−352 nm (Table 4). This shift confirms that these MD*n*−COOH ($n = 1-3$) molecules show enhanced intermolecular interaction of thiophene branches in the solid

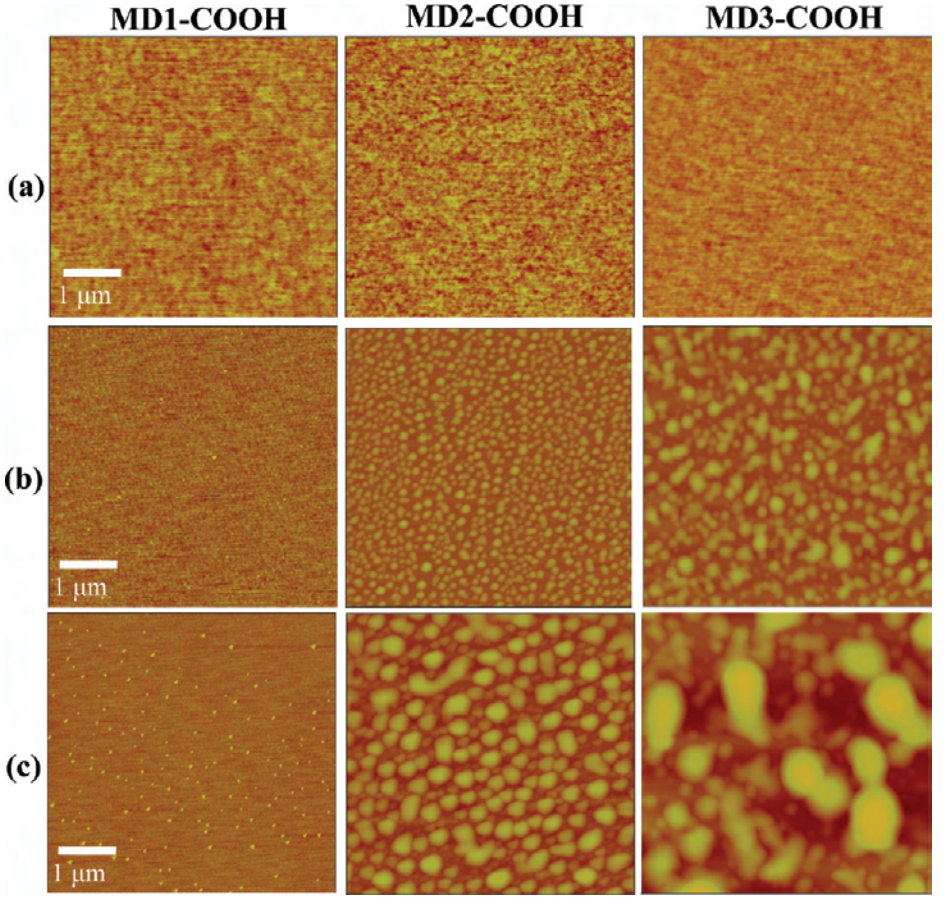

Figure 15. AFM topographical images of MD*n*−COOH LB films (n = 1−3) at P = 5 mN/m, for (a) 1 layer, (b) 5 layers, and (c) 11 layers. The Z scale is 200 nm.

state. At P = 20 mN/m, following monolayer collapse, the position of UV absorption maximum for MD1−COOH significantly red shifts even more, but for MD2−COOH and MD3−COOH, it is maintained (Table 4). At this point, the globular aggregates observed for collapsed monolayers are composed of weakly interacting MD*n*−COOH molecules in random conformation (Figure 14). A significant shift in the UV/vis absorption peak is usually observed for π-conjugated polymer systems that exhibit strong intermolecular interactions as a result of planarization of the molecular backbones organized in close $\pi-\pi$ stacks in the condensed, highly crystalline state.[52] However, a modest red shift observed in the case of condensed Langmuir monolayer (within 4−17 nm) indicates only modest densification of thiophene branches with the unlikely formation of $\pi-\pi$ stacks and, thus, very limited or no intramonolayer crystallization. In contrast to the 0th generation monodendron, the photo-emission measurement unfortunately did not show discernible spectra for the high generation monodendrons in the solid state, MD*n*−COOH (n = 1−3). This is consistent with the spin-coated films, as discussed earlier.

Finally, LB deposition of COOH-containing monodendrons resulted in consistent linear thickness growth only for MD2−COOH and MD3−COOH generations, and the subsequent layers were not transferrable for MD1−COOH when multilayered deposition was attempted (Figure 15 and Table 5). The increment per layer is close to the molecular dimension (~3 nm), indicating a consistent amount of materials added at each deposition cycle. However, a dramatic increase in surface micro-

Table 5. Measured Film Thickness for Multilayer MD*n*−COOH LB Films

sample names	thickness of multilayer LB films (nm)[a] 1 layer	5 layers	11 layers	rms roughness (nm)[b]
MD1−COOH	3.2	2.2	2.8	0.1
MD2−COOH	4.6	6.7	31.5	15.4
MD3−COOH	3.1	12	34.3	29.9

[a] Deposition surface pressure is P = 5 mN/m. [b] Roughness is for 11 layers (5 × 5 μm^2).

roughness indicates significant dewetting because of the poor intermolecular interactions between successive layers.

Conclusions

In conclusion, we observed that the fluorescence peak of MD*n* monodendrons in dilute solution progressively blue shift with increasing generation, indicating a somewhat distorted packing of branched thiophene fragments with an increasing number of junctions. In contrast, functionalized MD*n*−COOH monodendrons showed a progressive red shift with the increasing generation number, indicating gradual domination of $\sigma-\pi$ interactions and increasing the conjugation length. Moreover, the introduction of a carboxylic group resulted in the formation of a highly crystalline state of linear molecule (0th generation) with separated alkyl tail−thiophene packing, resulting in limited $\pi-\pi$ interactions, and thus, MD0−COOH monodendrons exhibit discernible photoluminescence in the solid state. On the other hand, the photoluminescence measurement of all other monodendron derivatives showed nondiscernible spectra in the solid state.

(52) Kokubo, H.; Sato, T.; Yamamoto, T. *Macromolecules* **2006**, *39*, 3959.

We demonstrated that adding branched thiophene fragments in the COOH-containing compounds resulted in achieving hydrophobic−hybrophilic balance sufficient to form stable, uniform, and elastic Langmuir monolayers with the thickness of 2−3 nm at the air−water at a modest surface pressure (< 10 mN/m) easily transferrable to a solid substrate. However, further increasing the thickness of the surface layers and the fabrication of ultrathin films (from tens to hundreds of nanometers) via multilayer LB deposition or spin casting is limited by the dewetting and the formation of globular surface aggregates on top of the first monolayer because of strong intermolecular interactions. A modest red shift observed for condensed Langmuir monolayers (below 18 nm) indicates minor densification of thiophene branches and limited intramonolayer crystallization and, thus, potential for the preservation of high photoluminescence. In contrast, thicker surface films showed a very significant red shift, confirming a dense molecular packing with strong $\pi-\pi$ interactions, which results in strong photoluminescence quenching.

Acknowledgment. This work is supported by NSF-DMR Grant 0756273 and RFBR Grant 07-03-01037. Authors thank Dr. N. M. Surin (ISPM RAS) for UV/vis investigations, Dr. M. I. Buzin (INEOS RAS) for DSC measurements, and Drs. A. P. Pleshkova (INEOS RAS) and I. Leschiner (Chemistry Department of MSU) for MALDI−TOF measurements.

Supporting Information Available: DSC curves for MD*n* and MD*n*−COOH (Figure S1), DSC curves for MD0 and MD0−COOH (Figure S2), and TOPM images of MD0−COOH (Figure S3). This material is available free of charge via the Internet at http://pubs.acs.org.